Electronic Supplementary Material (ESI) for Materials Advances.

Electronic Supplementary Information

In situ formation of robust nanostructured Cobalt oxyhydroxide / Cobalt oxide oxygen evolution reaction electrocatalysts

Yupeng Zhao, Dandan Gao, Johannes Biskupek, Ute Kaiser, Rongji Liu*, Carsten Streb*

Instrumentation and experimental section:

Powder X-ray diffraction (pXRD): Rigaku XRD-6000 diffractometer under the following conditions: 40 kV, 40 mA, CuKα radiation (λ = 0.154 nm).

Scanning electron microscopy (SEM): Hitachi 5200 SEM. Samples were measured at 10 kV acceleration voltage.

Transmission electron microscopy (TEM) and energy-dispersive X-ray spectroscopy (EDX): The samples were dispersed in ethanol and dropped casted to holey carbon support grids prior to TEM investigations. HRTEM images and diffraction patterns were acquired using a FEI Titan 80-300 equipped with an image-side aberration corrector, operated at 80 kV. A Thermo Fisher Talos 200X equipped with a SuperX EDX detector, operated at 200 kV in scanning (S) TEM mode was used for HAADF imaging and acquisition of elemental maps.

X-ray photoelectron spectroscopy (XPS): Monochromatized Al Kα exciting X-radiation using a PHI Quantera SXM system. The binding energies were calibrated based on C1s (284.8 eV).

Electrochemical measurements: Ametek workstation equipped with PMC 2000A and PMC 1000 channels in three-electrode setup (working electrode: a glassy carbon rotating disk electrode (RDE, disk surface area is 0.196 cm^2) and a rotating Pt ring-glassy carbon disk electrode (RRDE, carbon disk with the surface area of 0.2475 cm^2 surrounded by a Pt ring with a surface area of 0.1866 cm^2), reference electrode: Hg/HgO electrode, counter electrode: graphite rod) in 30 ml 1 M aqueous KOH electrolyte.

Polarization curves: recorded by linear sweep voltammetry (LSV) with the scan rate of 5 $mV \cdot s^{-1}$. All potentials were converted to the reversible hydrogen electrode (RHE) according to the Nernst equation ($E_{RHE} = E_{Hg/HgO} + E^0_{Hg/HgO} + 0.059\ V \times pH$).

Reaction pathway: The reaction pathway of OER was determined by detecting the formation of HO_2^- using an RRDE electrode. In this case, the current in the ring was recorded with the potential being held constantly at 1.5 V to oxidize HO_2^- intermediates in the Argon-saturated 1

M aqueous KOH solution. At the disk electrode, LSV was performed between 1.2-1.8 V at a scan rate of 5 $mV \cdot s^{-1}$.

Faradaic efficiency: Faradaic efficiency was calculated based on RRDE experiments, where a constant potential (1.5 V) was applied at the disk electrode to perform OER, while the ring electrode was held at a constant potential (0.4 V) to reduce the O_2 produced by OER. The electrolyte was saturated with Argon before the experiment. The faradaic efficiency (FE) was calculated with the following equation.

$$FE=I_{ring}/(I_{disk} \times N)$$

where I_{ring} and I_{disk} are the currents of the ring and disk, respectively. N is the current collection efficiency (here: 15.7%) of the RRDE.

Fabrication of working electrodes: 5 mg of composite and 30 µL of Nafion solution (5 wt%) were dispersed in 950 µL of ethanol, and 20 µL of deionized (DI) water, followed by ultrasonication for 1 h. 11.76 µL or 14.85 µL of the catalyst dispersion was deposited on the disk surface of an RDE or RRDE electrode (loading density of 0.3 $mg \cdot cm^{-2}$) and dried naturally at room temperature.

Electrochemically Active Surface Area (ECSA): ECSAs for each material were estimated by determining the electrochemical double-layer (C_{dl}) capacitance of the catalytic surface using cyclic voltammograms (CVs) in a potential range of 0.75V - 0.99 V where no redox-processes occur. Before the CV data was collected, working electrodes were scanned for several potential cycles to stabilize the signals. There is a linear relationship between half of the current density difference (at 0.87 V) and the scan rate, the slope is the C_{dl}.

Electrochemical impedance spectroscopy (EIS): EIS of the catalysts was recorded at a potential of 1.55 V vs. RHE with an AC amplitude of 5 mV by sweeping the frequency from 100 kHz to ~0.01 Hz. All samples were recorded under identical experimental conditions.

Analytical section

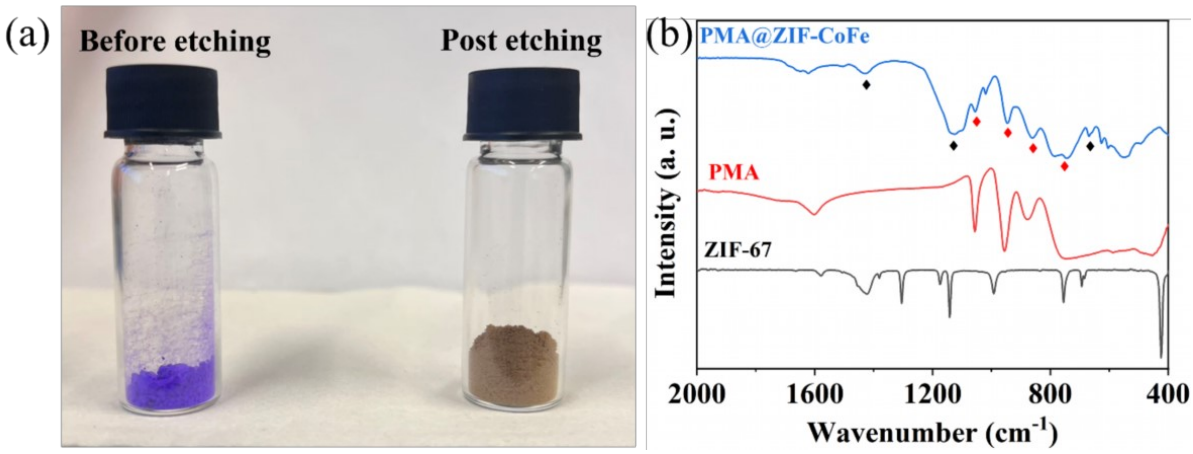

Figure S1. (a) The optical photographs of ZIF-67 and PMA@ZIF-CoFe. (b) FTIR spectra of ZIF-67, PMA, and PMA@ZIF-CoFe. The peaks labeled in red and black in PMA@ZIF-CoFe are assigned to PMA and ZIF-67, respectively. It indicates the presence of $[PMo_{12}O_{40}]^{3-}$ in ***Composite 1.***

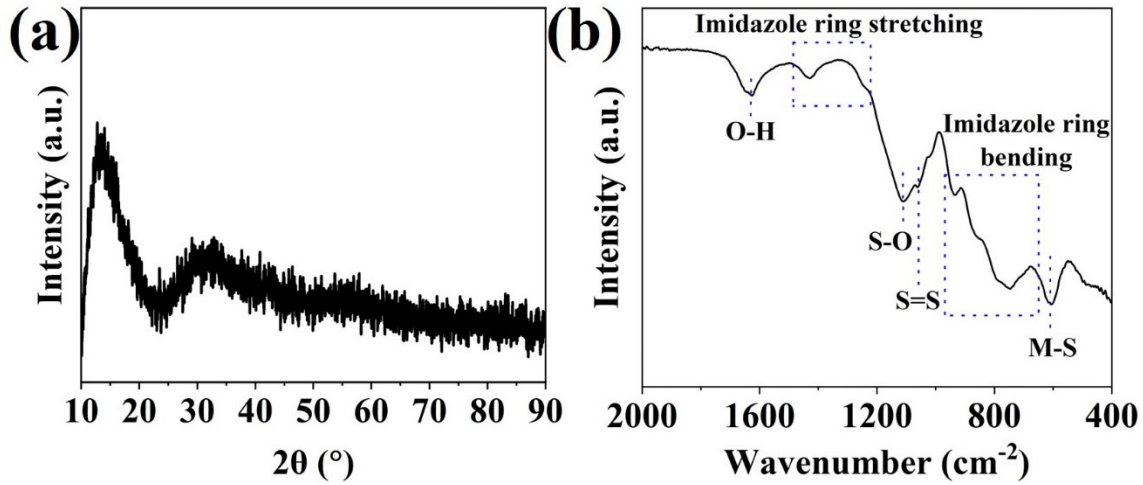

Figure S2. (a) pXRD data and FT-IR spectrum of ***Composite 2***. The broad peaks in pXRD pattern at 13.8° and 30.8° are assigned to polymethyl methacrylate (PMMA),[1,2] which serves as the pXRD sample holder.

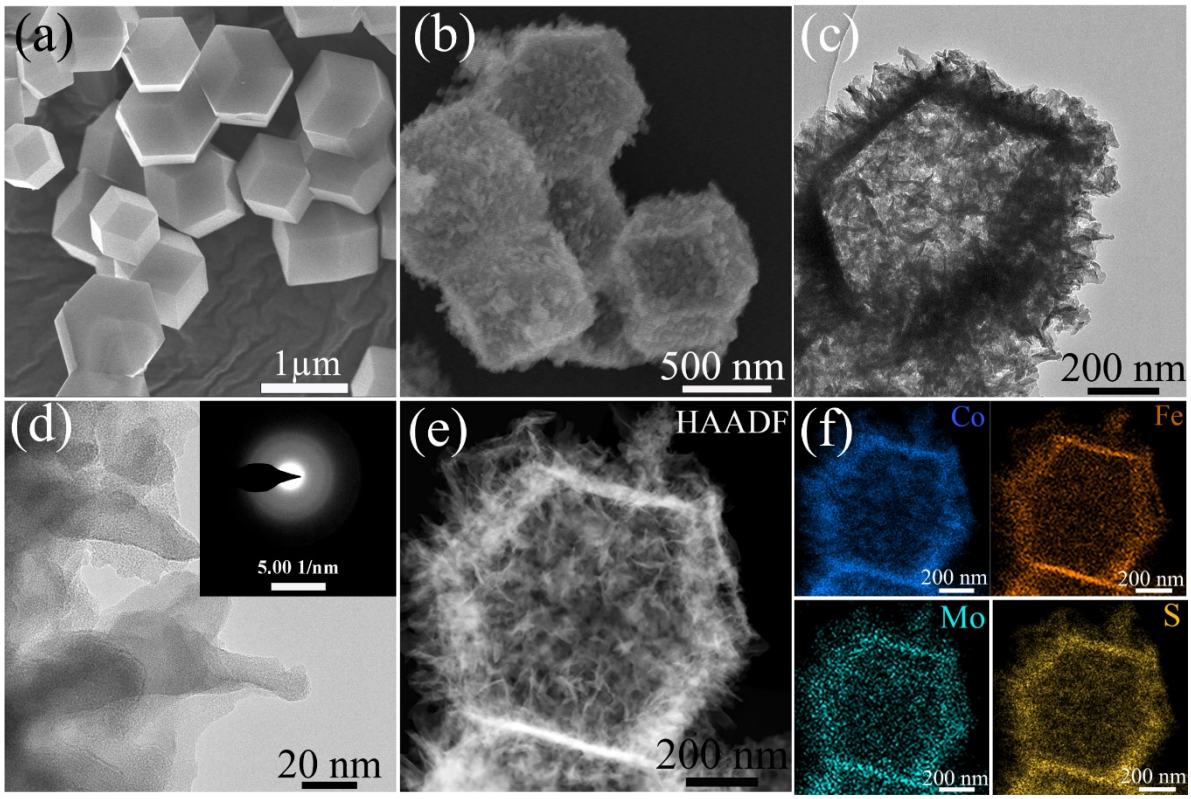

Figure S3. SEM images of (a) ZIF-67, and (b) ***Composite 2***. (c and d) TEM and HRTEM images with the insert of SAED pattern. (e and f) STEM high angle annual dark-field STEM image and corresponding EDX elemental mappings.

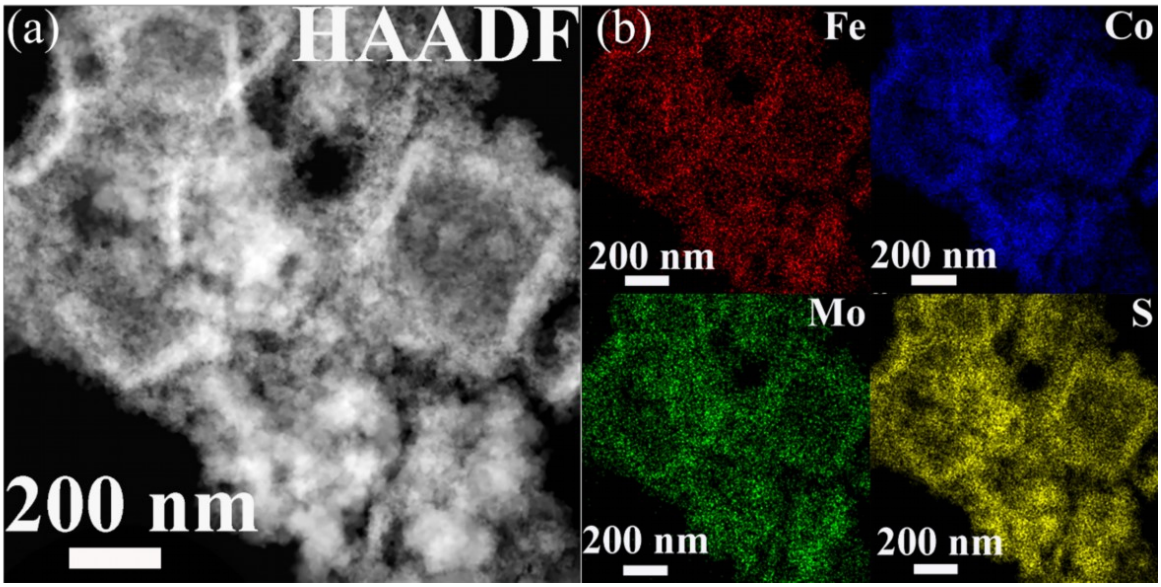

Figure S4. HAADF-HRTEM image (a) of ***Composite 1*** and corresponding STEM-EDX elemental mappings (b) of Fe, Co, Mo, and S

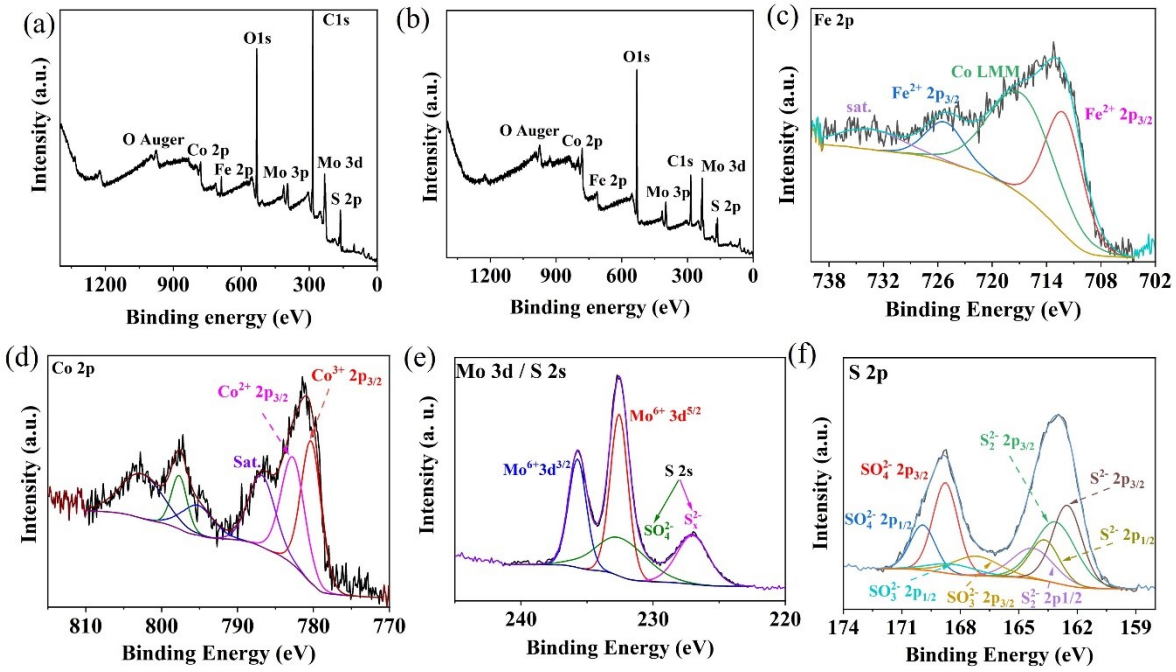

Figure S5. Overview XPS spectra of ***Composite 1*** (a) ***Composite 2*** (b), and deconvoluted high-resolution spectra of Fe 2p (c), Co 2p (d), Mo 3d (e), and S 2p (f) of ***Composite 2.***

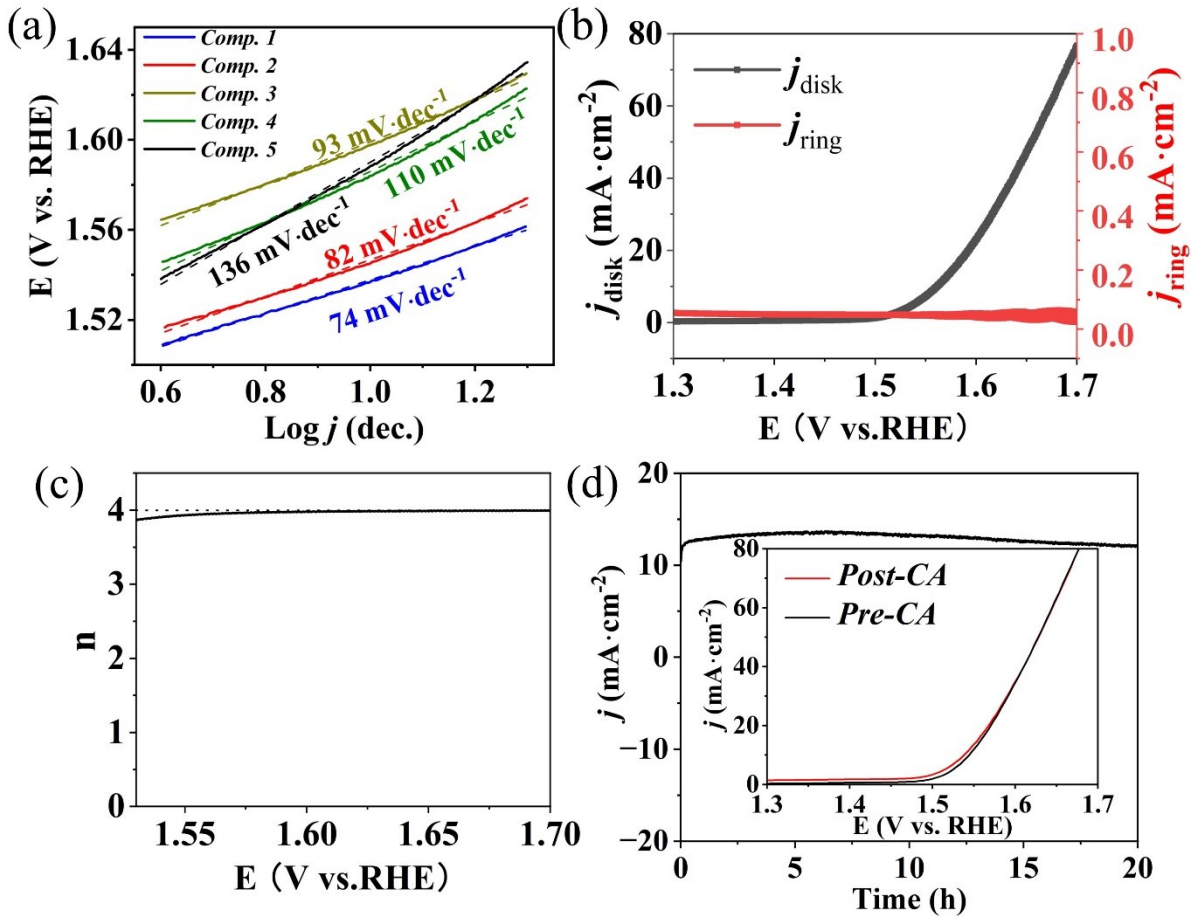

Figure S6. (a) Tafel plots of ***Composite 1***, ***Composite 2***, and reference composites. (b) Ring and disk current density of ***Composite 1*** on an RRDE (1600 rpm) in Argon-saturated 1M KOH solution, disk electrode was set LSV scan from 1.3 V to 1.7 V, while the ring electrode (at 1.5 V vs RHE) was used to detect any peroxide formation. (c) Electron transfer number calculated from the equation $\boldsymbol{n} = 4 \times \frac{I_d}{\frac{I_r}{N} + I_d}$. (d) Chronoamperometry curves at η = 330 mV without iR compensation (insert: LSV polarization curves comparison before and after 20 h stability test) of ***Composite 1***.

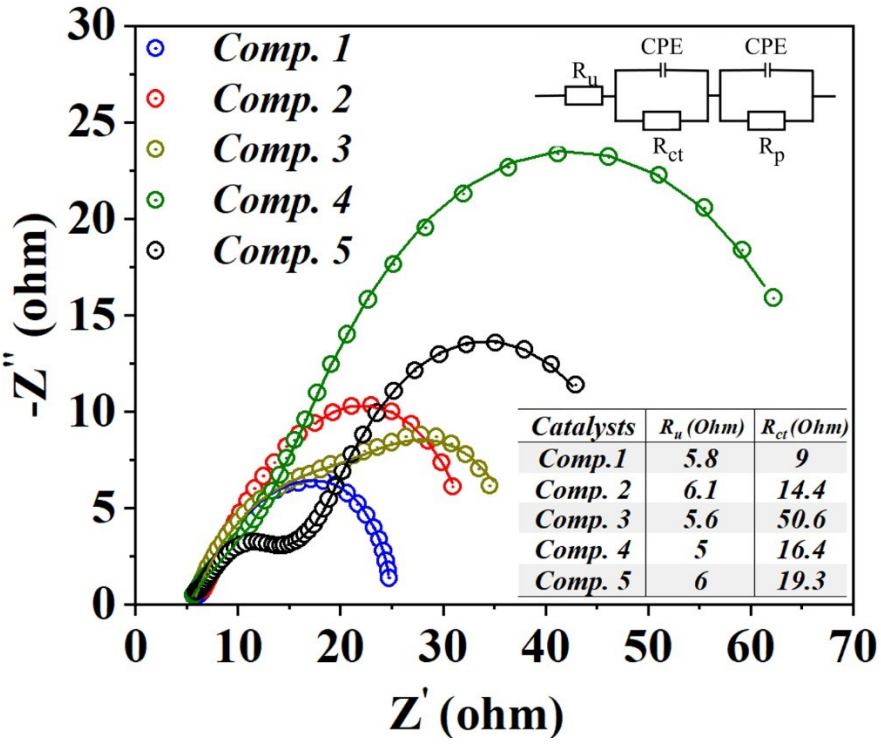

Catalysts	R_u (Ohm)	R_{ct} (Ohm)
Comp.1	5.8	9
Comp. 2	6.1	14.4
Comp. 3	5.6	50.6
Comp. 4	5	16.4
Comp. 5	6	19.3

Figure S7. Electrochemical impedance spectroscopy (EIS, Nyquist plots) measured at the overpotential of 300 mV, (circles represent the experimental data, lines are the data fitting based on the equivalent circuit (insert)). The semicircles in the high-frequency range of the Nyquist plots are assigned to solution resistance (R_u), charge transfer processes (R_{ct}) and diffusion/adsorption of reaction intermediates due to slow diffusion through the reaction interface (R_p). CPE (constant phase element) is the double-layer capacitance. [3]

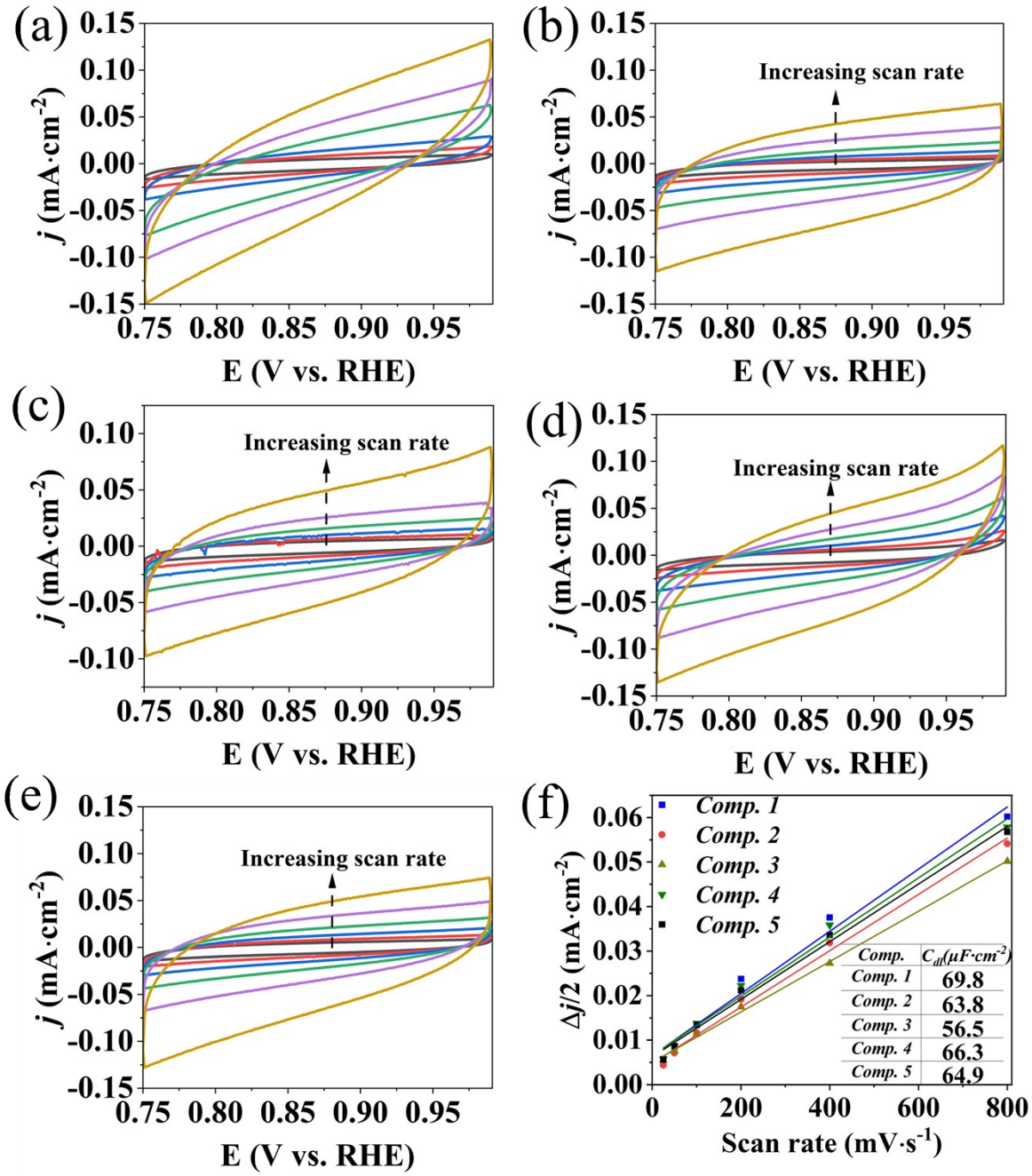

Figure S8. Double-layer capacitance measurements for determining electrochemically active surface area of different Composites. Cyclic voltammetry (a-e) scanned from 0.82 to 0.92 V vs. RHE with the scan rates from 25 to 800 mV·s^{-1} and (f) half of the capacitive current density ($\Delta j/2$) at 0.87 V vs. RHE as a function of the scan rates of ***Composite 1***, ***Composite 2***, ***Composite 3***, ***Composite 4***, and ***Composite 5***, respectively.

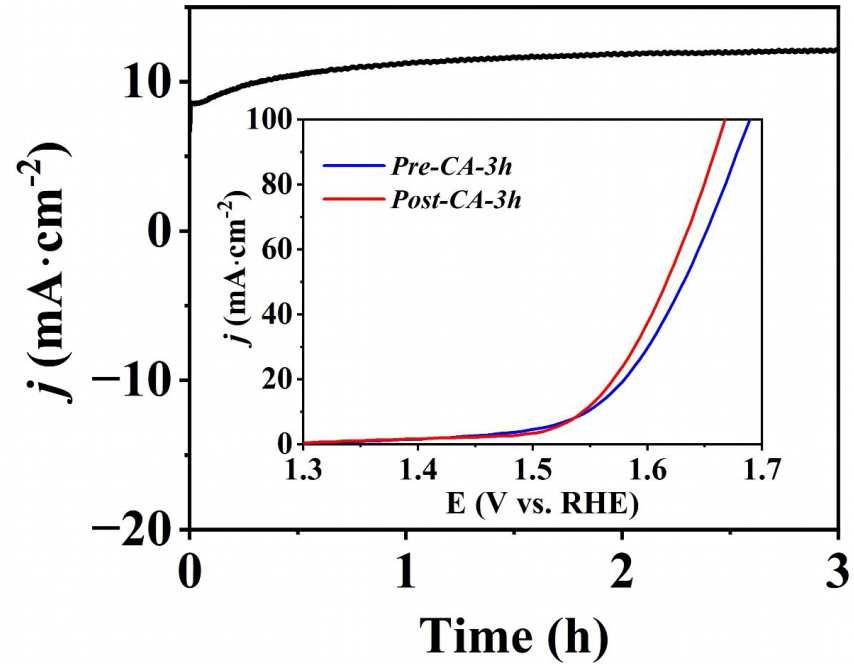

Figure S9 Chronoamperometry curves at η = 330 mV without iR compensation (insert: LSV polarization curves comparison before and after 3 h stability test).

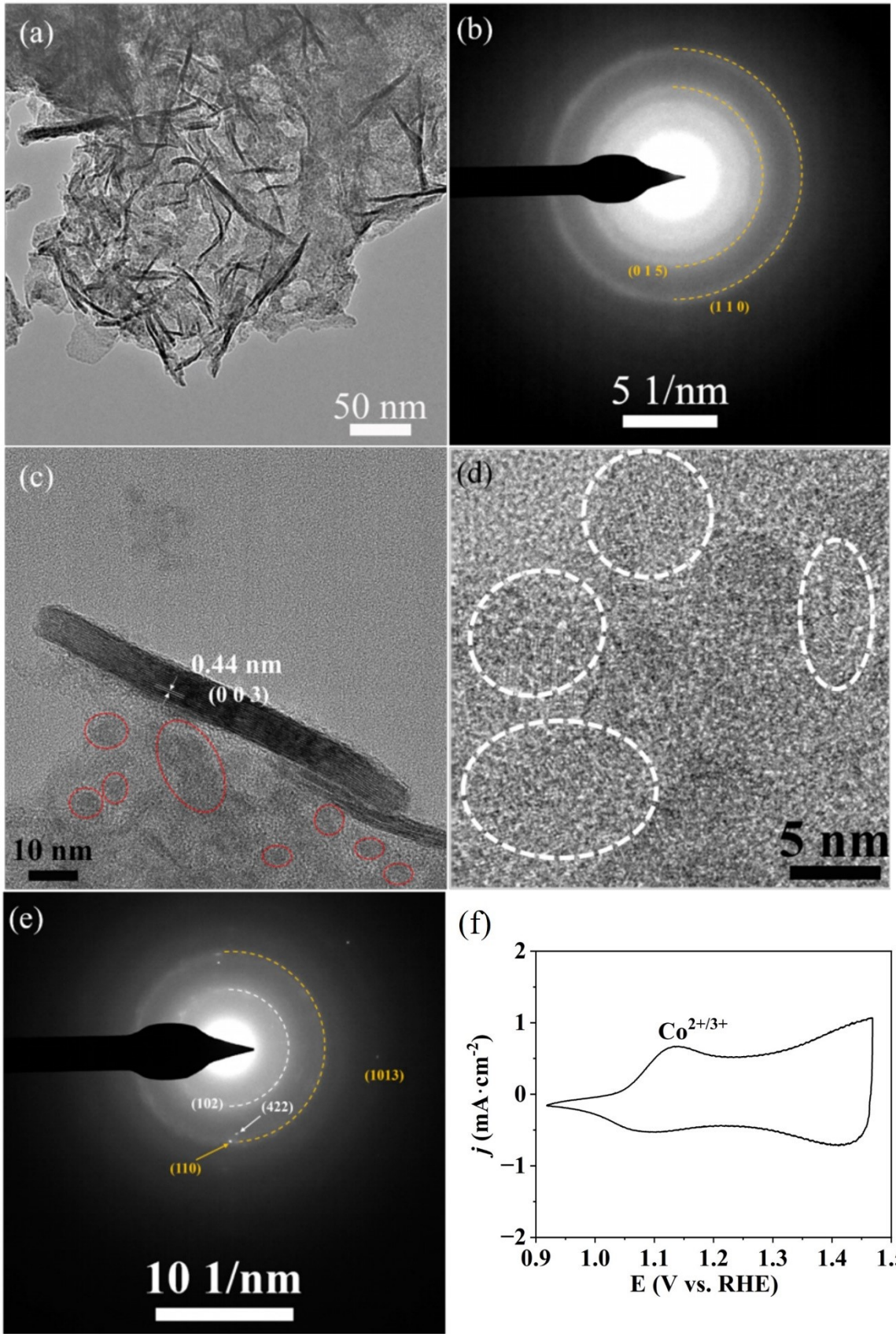

Figure S10 HR-TEM images and corresponding SAED pattern of ***Composite 1*** after electrocatalysis for 3 h (a, b) and 10 h (c - e). (f) Cyclic voltammetry before CA test at the scan rate of 100 mV/s of ***Composite 1*** in 1 M KOH solution.

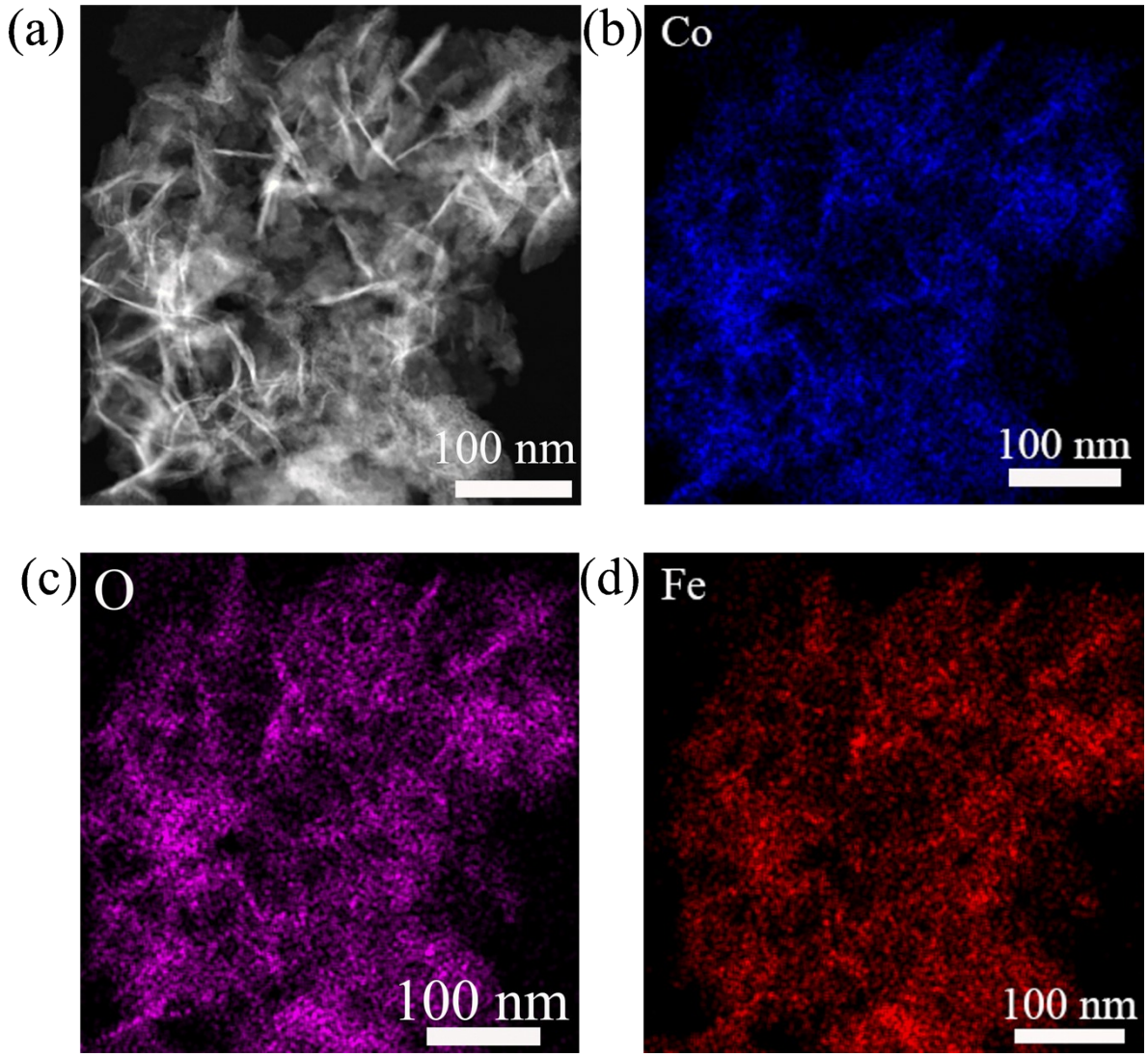

Figure S11 Compositional analysis of ***Composite 1*** post catalysis for 3 hours: (a) High angle annular dark-field STEM image and corresponding elemental mappings (b-d) using EDX.

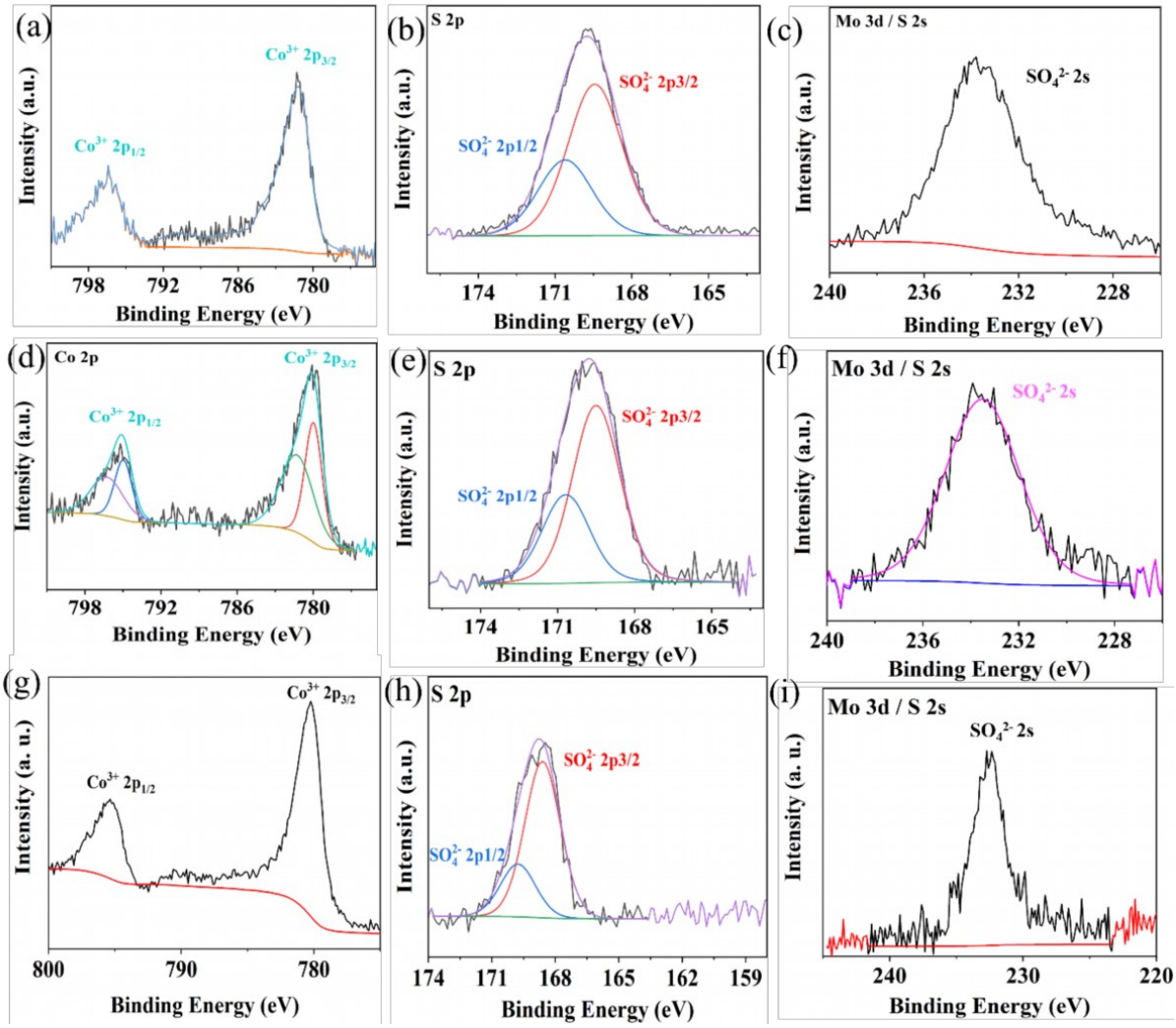

Figure S12 Deconvoluted high-resolution spectra of ***Composite 1*** after electrocatalysis for 3 h (a-c), 10 h (d-f), and ***Composite 2*** after electrocatalysis for 10 h (g-i)

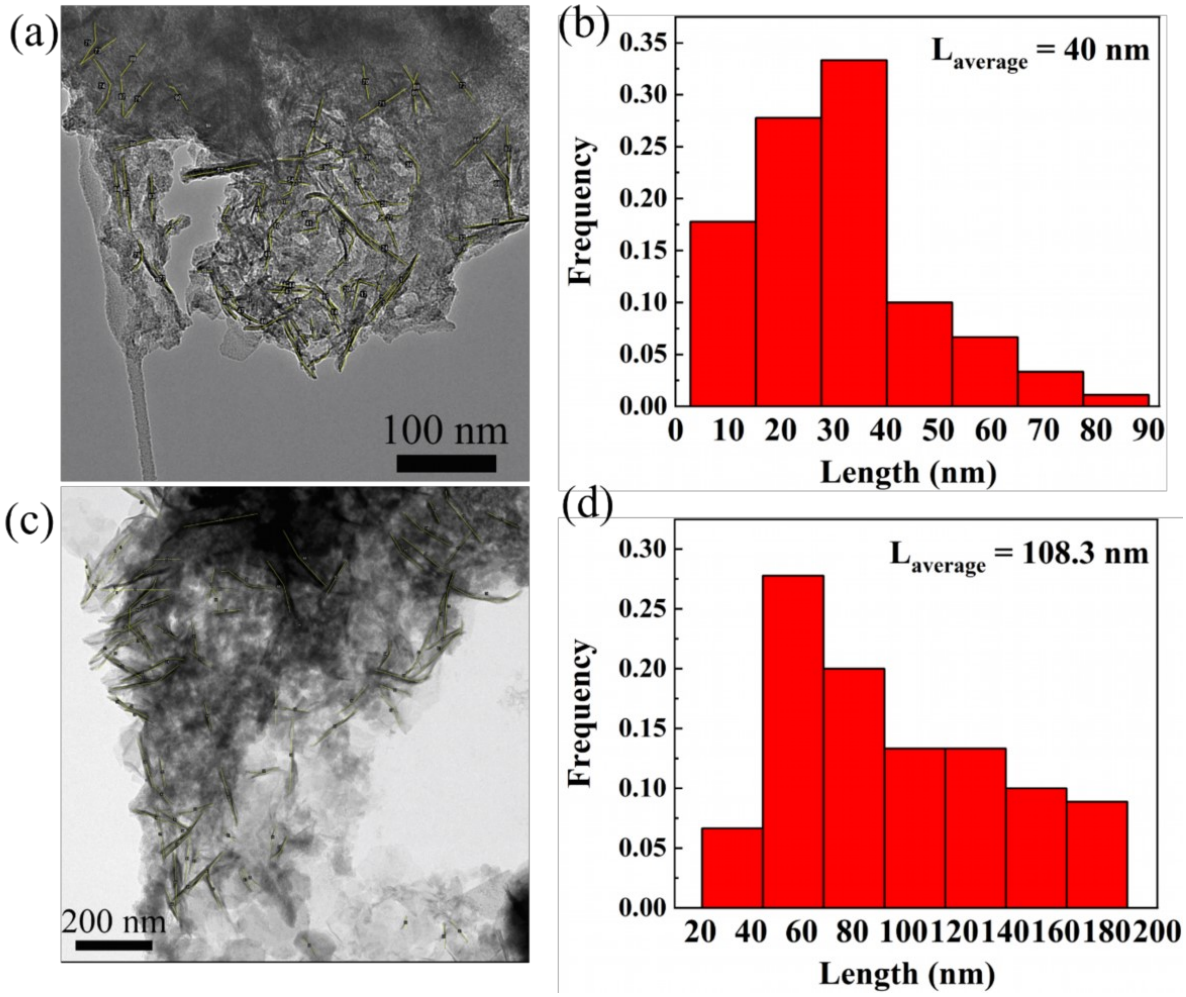

Figure S13 TEM images of ***Composites 1*** post electrocatalysis for 3 hours (a) and 10 hours (c), and the corresponding nanofibers length distribution (b and d)

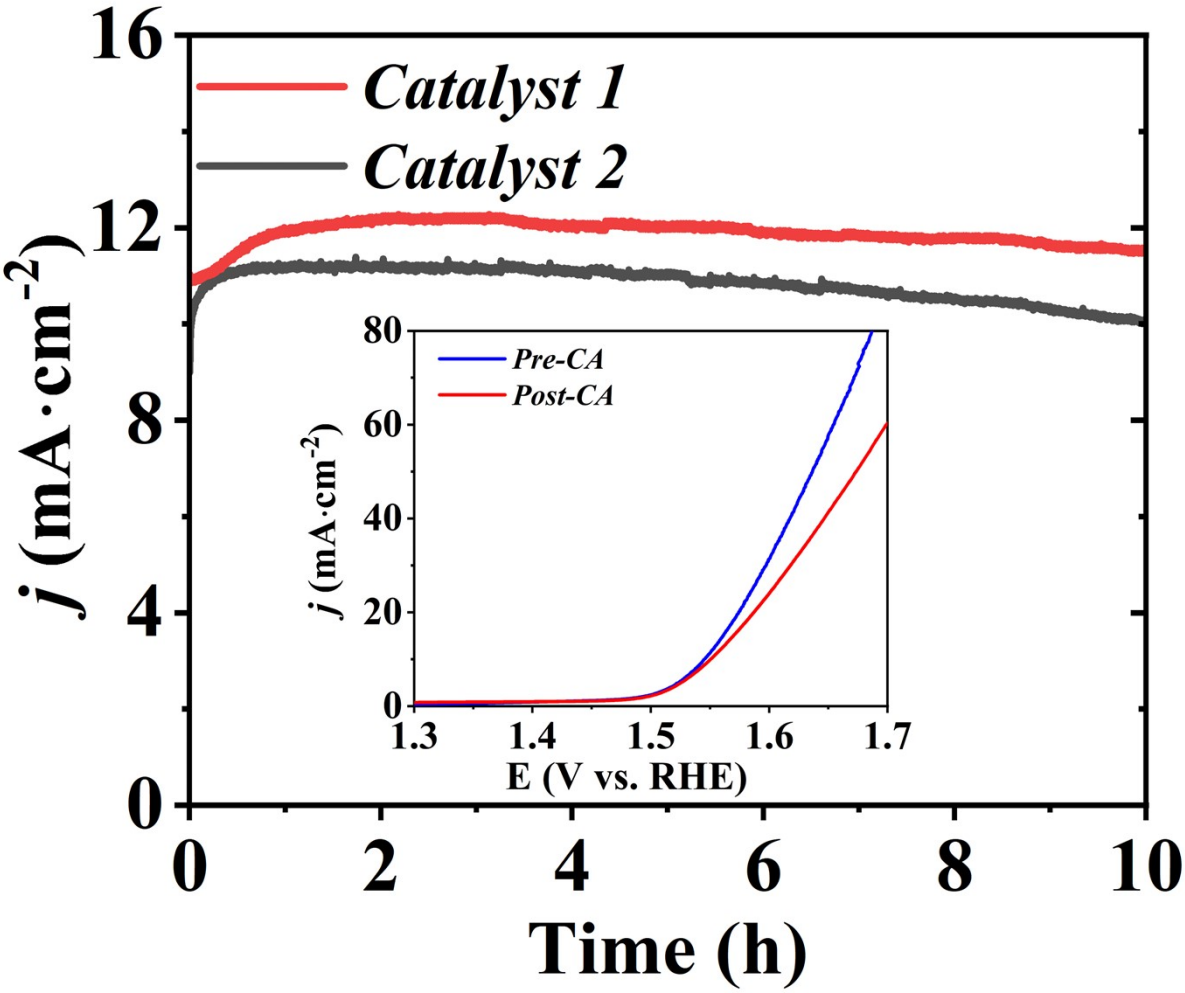

Figure S14 Chronoamperometry curves at η = 330 mV without iR compensation of ***Composite 1*** and ***Composite 2***. (Insert: LSV polarization curves comparison before and after 10 h stability test of ***Composite 2***).

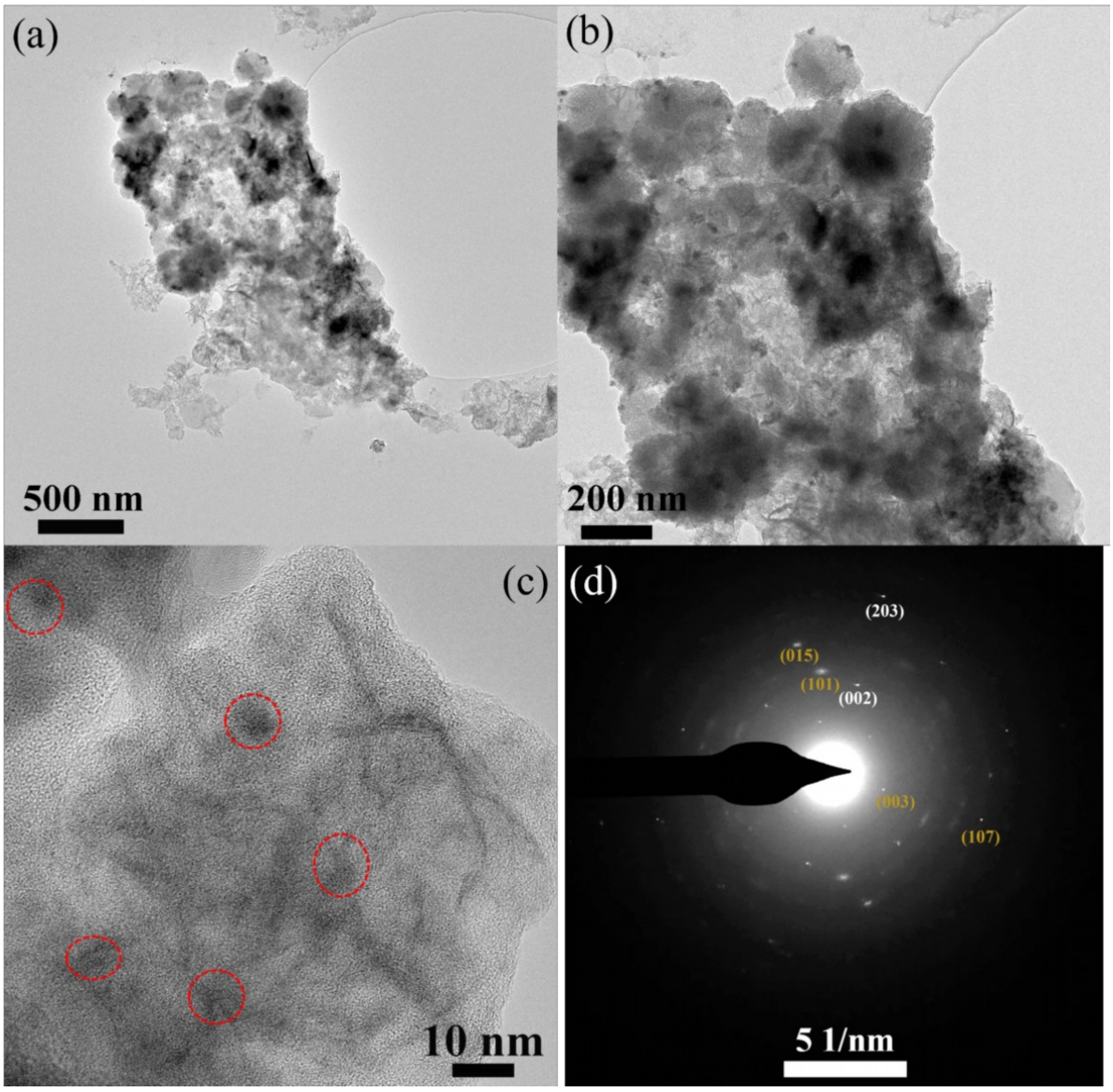

Figure S15. Post-catalysis structural and compositional analysis of ***Composite 2***: (a, b) TEM images, (c) HRTEM image, and (d) corresponding SAED pattern after long-term catalysis

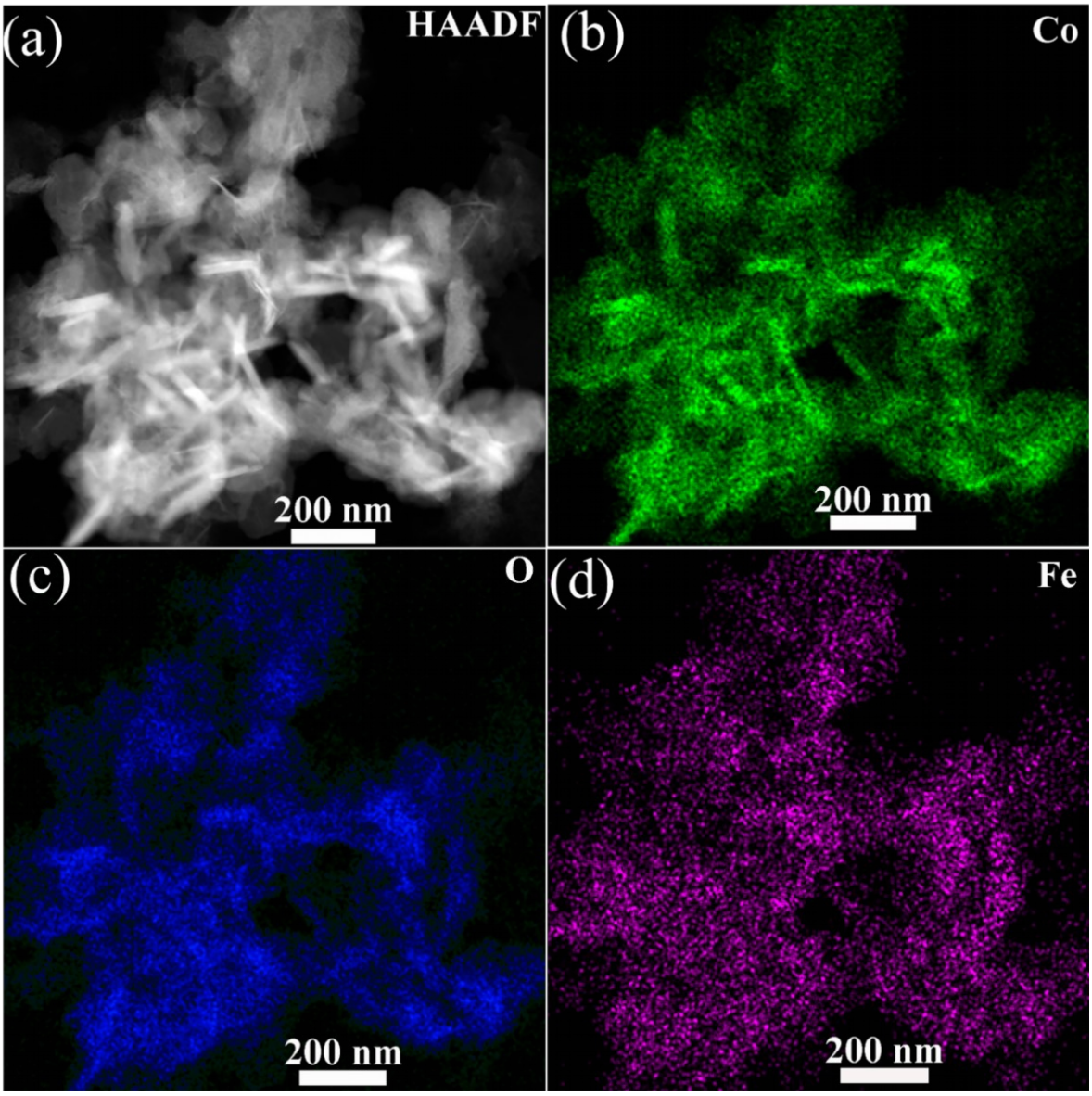

Figure S16. Compositional analysis of ***Composite 1*** post catalysis for 10 hours: (a) High angle annular dark-field STEM image and corresponding elemental mappings (b-d) using EDX.

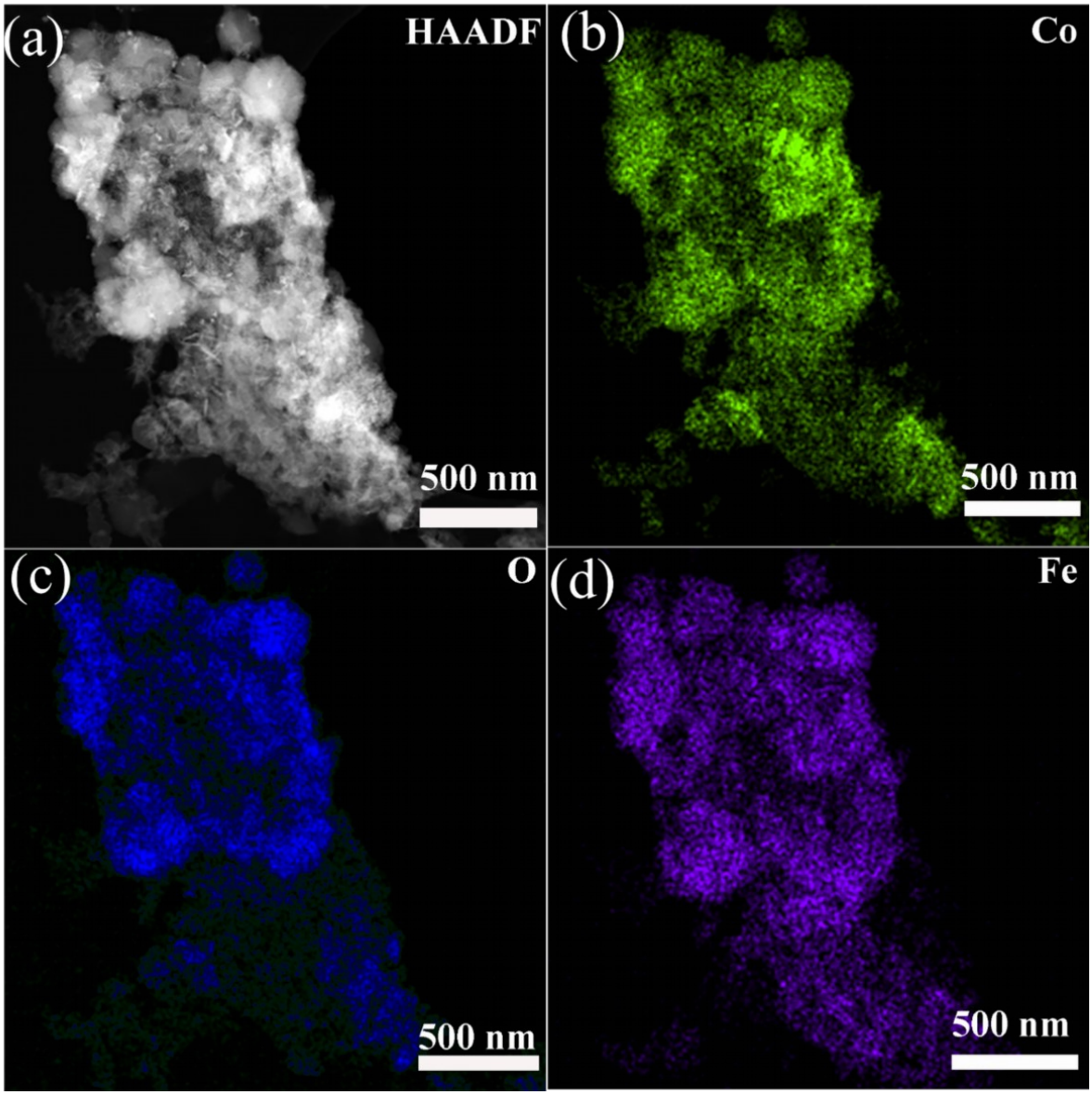

Figure S17. Post-catalysis compositional analysis of ***Composite 2***: (a) High angle annular dark-field STEM image and corresponding elemental mappings (b-d) using EDX

Reference

[1] M. Hashem, M. F. Al Rez, H. Fouad, T. Elsarnagawy, M. A. Elsharawy, A. Umar, M. Assery, S. G. Ansari, *Sci Adv Mater* **2017**, *9*, 938–944.

[2] F. Yousefi, S. B. Mousavi, S. Z. Heris, S. Naghash-Hamed, *Scientific Reports 2023 13:1* **2023**, *13*, 1–19.

[3] G. Li, L. Anderson, Y. Chen, M. Pan, P. Y. Abel Chuang, *Sustain Energy Fuels* **2017**, *2*, 237–251.